



HAL
open science

Demagnetization of transmitted electrons through a quasi-perpendicular collisionless shock

Philippe Savoini, M. Balikhin, S. Walker, V. Krasnoselskikh, Bertrand Lembège

► **To cite this version:**

Philippe Savoini, M. Balikhin, S. Walker, V. Krasnoselskikh, Bertrand Lembège. Demagnetization of transmitted electrons through a quasi-perpendicular collisionless shock. *Journal of Geophysical Research*, 2003, 108 (A6), 10.1029/2002JA009288 . insu-03038933

HAL Id: insu-03038933

<https://insu.hal.science/insu-03038933>

Submitted on 3 Dec 2020

HAL is a multi-disciplinary open access archive for the deposit and dissemination of scientific research documents, whether they are published or not. The documents may come from teaching and research institutions in France or abroad, or from public or private research centers.

L'archive ouverte pluridisciplinaire **HAL**, est destinée au dépôt et à la diffusion de documents scientifiques de niveau recherche, publiés ou non, émanant des établissements d'enseignement et de recherche français ou étrangers, des laboratoires publics ou privés.

Demagnetization of transmitted electrons through a quasi-perpendicular collisionless shock

B. Lembège and P. Savoini

Centre d'Etude des Environnements Terrestre et Planétaires/Université de Versailles Saint-Quentin-en-Yvelines (CETP/UVSQ), Vélizy, France

M. Balikhin and S. Walker

Department of Automatic Control and Systems Engineering, University of Sheffield, Sheffield, UK

V. Krasnoselskikh

Laboratoire de Physique et Chimie de l'Environnement, CNRS, Orléans la Source, France

Received 30 January 2002; revised 23 December 2002; accepted 20 February 2003; published 26 June 2003.

[1] Physical processes responsible for the electron demagnetization within the front of a quasiperpendicular collisionless shock are analyzed via a comparative study between theoretical calculations and computer simulations. Herein, simulation results of a shock in supercritical regime are based on the use of a 2-D full particle self-consistent code. Present statistics on the spatial widths of the magnetic field (L_{Br}) and electric field (L_{Er}) within the ramp show that their ratio $R = L_{Er}/L_{Br}$ is around 1; this value is appropriate to demagnetize electrons and to provide a resulting deviation from adiabaticity [Balikhin *et al.*, 1998]. In order to verify this theoretical expectation, two complementary approaches are used. First, the deviation of the full electron gyroperiod from the magnetic gyroperiod is analyzed from the trajectories of “marked” self-consistent electrons crossing the shock ramp. In such a case, nonstationary and nonuniformity effects of the shock front are fully involved. Second, such effects are removed and test particles simulations are used in order to determine the strength of electron demagnetization when effects of width shock along the shock normal are included only. Both approaches confirm that demagnetization takes place within the first half of the ramp, that is, where the gradient dE_{ix}/dx seen by transmitted electrons is positive. Statistical results performed using test particles simulations show that a noticeable number of demagnetized electrons are formed within the ramp even for a moderate supercritical Mach number and that the relative percentage of demagnetized/magnetized electrons varies according to the nonstationary behavior of the shock front (self-reformation). **INDEX TERMS:** 7851 Space Plasma Physics: Shock waves; 7843 Space Plasma Physics: Numerical simulation studies; 7514 Solar Physics, Astrophysics, and Astronomy: Energetic particles (2114); 6939 Radio Science: Magnetospheric physics; **KEYWORDS:** collisionless shocks, particle demagnetization, adiabatic/nonadiabatic electrons, terrestrial bow shock

Citation: Lembège, B., P. Savoini, M. Balikhin, S. N. Walker, and V. V. Krasnoselskikh, Demagnetization of transmitted electrons through a quasi-perpendicular collisionless shock, *J. Geophys. Res.*, 108(A6), 1256, doi:10.1029/2002JA009288, 2003.

1. Introduction

[2] The problem of investigating the electron heating mechanisms that exist within the front of quasiperpendicular shocks is closely related to the definition of the scales of the shock front structure. The primary question is whether the heating mechanism is related to the presence of the turbulence in the foreshock region or in the vicinity close to the shock front. Previous analytical [Goodrich and Scudder, 1984] and simulation results [Veltri *et al.*, 1990; Savoini and Lembège, 1994] have unambiguously shown that the electron heating, which takes place at the shock front, is due to

the macroscopic fields at shock front rather than due to plasma turbulence whose effectiveness was shown to bring a second-order contribution. These simulations were performed using both Monte Carlo codes [Veltri *et al.*, 1990], in which the particles interact with prescribed B fields, and 1-D and 2-D full particle codes [Savoini and Lembège, 1994], in which self-consistent interactions between the waves and particles were fully included. However, the question of breakdown in adiabaticity was not considered at that time. Using Monte Carlo simulations, Veltri and Zimbardo [1993a, 1993b] have shown that when letting electrons propagate in drift approximation in electric and magnetic fields profiles derived from data, it was not possible to account for the observed perpendicular temperature also when electrostatic turbulence described in the same approx-

imation was taken into account. The perpendicular temperature could be explained by introducing the effects of electrons interactions with whistler waves, thus breaking the drift approximation.

[3] Since the turbulence is not the major factor, the answer to the question of whether the heating is adiabatic or not is associated with the macroscopic structure of the shock front, namely, the relative values of several characteristic scales [Balikhin *et al.*, 1998]. The most important scales are the spatial widths of the electric and magnetic fields within the ramp, and the local electron Larmor radius.

[4] From the early satellite measurements by Vela-4 satellite in the 60s, it was unambiguously demonstrated that the electron heating takes place on a very small spatial scale [Montgomery *et al.*, 1970]. A comprehensive statistical study of electron heating versus various shock parameters has been performed by Schwartz *et al.* [1988]. The main question to be addressed in this paper is to determine the real impact of the electric field gradients on electron heating. This question can be expressed in terms of corresponding scales in both the electric field variation and the increase of the electron heating observed at the shock front. The experimental determination of the DC electric field scale is difficult to measure because of fluctuations in the plasma potential. The quasi-absence of direct measurements makes the comparison of the macroscopic field scales with the electron heating scale quite difficult. There are several ways used by different authors to determine the DC electric field making use of the relationship between the different parameters, such as noncoplanar magnetic field component, or current layer properties with the variations in the electron distribution function as described in the two-fluid hydrodynamics [Scudder *et al.*, 1986a]. Such procedures correspond to indirect measurements of shock front scales and is based on certain assumptions. To our knowledge, the only two works based on direct measurements of the DC electric fields are those of Formisano [1982] and Heppner *et al.* [1977]. It is worth pointing out that Heppner *et al.* [1977] came to the conclusion that the spatial scales of the electric field can be as small as the electron inertial length c/ω_{pe} . Thus a comparative study of the scales of magnetic and electric field variations through the shock front is incomplete. However, such a comparative study can be performed with the help of computer simulations where all background fields and particle data are available and may be analyzed in detail. Full particle simulations, in which both electrons and ions scales are included, are quite appropriate to such a study since these allow to access to the self-consistent dynamics and to the scales of the various fields components. That is the first objective of our paper. The second objective is to use these results in order to identify whether deviation from adiabaticity takes place and at which precise location within the shock front it occurs. One key purpose is to analyze this deviation within the shock front itself in terms of electron demagnetization, rather than to estimate adiabaticity breakdown based upon the differences between upstream and downstream regions far from the shock front. Then, terms “magnetized” and “demagnetized” will be used in order to refer to the characteristic trajectories of electrons within the shock ramp. These labels are used in preference to “adiabatic” and “nonadiabatic” on the basis of the adiabatic momentum or on collective motion (heat-

ing) as used in previous works. In the purpose of this study, two complementary approaches are used. First, features of directly transmitted “marked” electrons are analyzed. The term “marked” is used to refer to small subset of electrons that have been selected among all particles involved in the self-consistent simulations. In this case, nonstationary and nonuniformity effects of the shock front are fully involved. In the second approach, basic mechanisms responsible for demagnetization are analyzed with test particle simulations, in which nonstationary and nonuniformity effects of the shock front have been removed. Moreover, statistical analysis will provide the relative percentage of magnetized and demagnetized electrons through different profiles of the shock front.

[5] The first evidence for strong nonadiabatic electron heating was demonstrated in simulations of a very high Mach number perpendicular shock by Tokar *et al.* [1986]. At that time, the precise reason of adiabaticity deviation was not identified yet. The present results show that such a deviation takes place even for moderate Mach number regime.

[6] The present study is organized as follows. Characteristics of the simulations performed herein are described in section 2. Numerical results providing the width scales determined from the profiles of magnetic and electric fields components are provided in section 3, in which comparison with previous works is also presented. Different levels of electron demagnetization identified from self-consistent simulations results are presented in section 4. Complementary test particle simulations results and associated statistical analysis are presented in section 5. Conclusions are summarized in section 6.

2. Conditions of Numerical Simulations

[7] The initial and boundary conditions used in the present 2-D electromagnetic full particle simulations are identical to those already explained in detail by Lembège and Savoini [1992] and Savoini and Lembège [1994]. Briefly, the planar shock is propagating along x axis while its front extends along y direction; nonperiodic conditions are applied along x axis while the code is periodic along y (Figure 1a). The static magnetic field B_o is directed out of the simulation plane (Figure 1b).

[8] All dimensionless quantities are indicated by a tilde (\sim) and are normalized as follows. The spatial coordinate is $\tilde{x} = x/\Delta$; velocity $\tilde{v} = v/\omega_{pe}\Delta$; momentum of species γ , $\tilde{p}_\gamma = p_\gamma/m_e\omega_{pe}\Delta$; electric field $\tilde{E} = qE/m_e\omega_{pe}^2\Delta$; magnetic field $\tilde{B} = qB/m_e\omega_{pe}^2\Delta$; time $\tilde{t} = \omega_{pe}t$. The parameters Δ , ω_{pe} , m_e , q and n_o are, respectively, the numerical grid spacing, the electron plasma frequency, the electron mass, the electric charge and the particle density at $t = 0$. The basic parameters are lengths $\tilde{L}_x = 4096$, $\tilde{L}_y = 128$; reflecting walls are located at $\tilde{x}_l = 2048$ and $\tilde{x}_r = 4096$; $\Delta\tilde{x}_{pulse} = 5$; velocity of light $\tilde{c} = 3$, mass ratio $m_e/m_i = 0.024$. At $t = 0$, the particle density is $n_e = n_i = 4$ at each grid point ($2/\Delta x$ and $2/\Delta y$), the temperature ratio $T_e/T_i = 1.58$ and the magnetic field $|\tilde{B}_o| = 1.5$. For these initial conditions the plasma parameters are summarized in Table 1 for both electrons and ions. The shock is propagating in a supercritical regime ($M_A = 3.2$, where $M_A = \tilde{v}_{sh}/\tilde{v}_A$) with an angle $\theta_o = 55^\circ$, where θ_o is the angle between the shock normal in the x -direction and

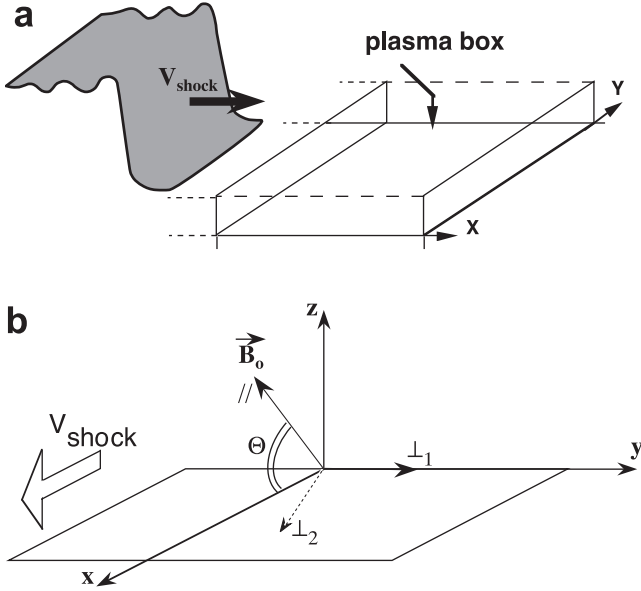


Figure 1. (a) Sketch of the two-dimensional simulation box (x,y) including the vacuum region and the plasma region; (b) reference set used in the simulation code; \vec{B}_0 is lying partially outside the simulation plane. Directions $//$, \perp_1 and \perp_2 are respectively defined with respect to the upstream magnetostatic field \vec{B}_0 .

the direction of the upstream magnetostatic field B_0 ; the Alfvén velocity $\tilde{v}_A = 0.23$ is determined from the upstream plasma parameters and \tilde{v}_{sh} is the shock velocity along x . The size of the box allows the shock and particles dynamics to be followed over a time $\tilde{t} \approx 3\tilde{\tau}_{ci}$ (or equivalently $18.75\tilde{\omega}_{ci}^{-1}$), where $\tilde{\tau}_{ci}$ is the upstream ion gyroperiod.

3. Numerical Results: Widths Scales of Magnetic and Electric Fields

[9] Similar full particle simulations performed previously with 1-D code [Biskamp and Welter, 1972; Lembège and Dawson, 1987] and 2-D code [Lembège and Savoini, 1992] have already shown the nonstationary character of the shock front. Two-dimensional simulations have been also used to analyze the nonuniformity of the shock front [Lembège and Savoini, 1992]. The present section is structured as follows: the nonstationarity and nonuniformity features of the shock front are shortly described (sections 3.1 and 3.2), the width scales of both electric and magnetic fields are directly determined from numerical results (section 3.3), and results are compared with previous simulations results (section 3.4) and with previous experimental observations (section 3.5).

3.1. Nonstationarity of the Shock Front

[10] Figure 2 shows a stackplot of the y -integrated space profile of the main magnetic field component B_{tz} at different times during the run where the well-known features of a quasi-perpendicular shock in supercritical regime, namely the foot, the ramp of the shock and the magnetic overshoot, which delimits the downstream region, are easily recognizable. The shock front is propagating from left to right. This figure clearly shows evidence for shock front reformation similar to that already shown in 1-D [Lembège and Dawson

Table 1. Upstream Plasma Parameters Defined for the 2-D Run

Parameter	Electrons	Ions	
\tilde{v}_{th}	thermal velocity	0.3	0.037
λ_D	Debye length	0.42	0.064
$\tilde{\rho}_c$	gyroradius	0.84	4.35
$\tilde{c}/\tilde{\omega}_p$	inertial length	3	19.4
$\tilde{\omega}_c$	gyrofrequency	0.5	0.012
$\tilde{\omega}_p$	plasma frequency	1	0.155
$\tilde{\tau}_{ci}$	gyroperiod	12.55	523.6
β		0.24	0.15

[1987] and 2-D [Lembège and Savoini [1992] simulations, which can be explained as follows. It is well known and evidenced also herein (but not shown in the current paper), that a percentage of upstream ions are reflected from the shock front and are responsible for the formation of the foot as observed in hybrid [Leroy et al., 1981], and full particle simulations [Biskamp and Welter, 1972; Lembège and Dawson [1987]. Their density is so high that the foot reaches an amplitude large enough to reflect incoming ions and to form a new shock front. This cyclic reformation of

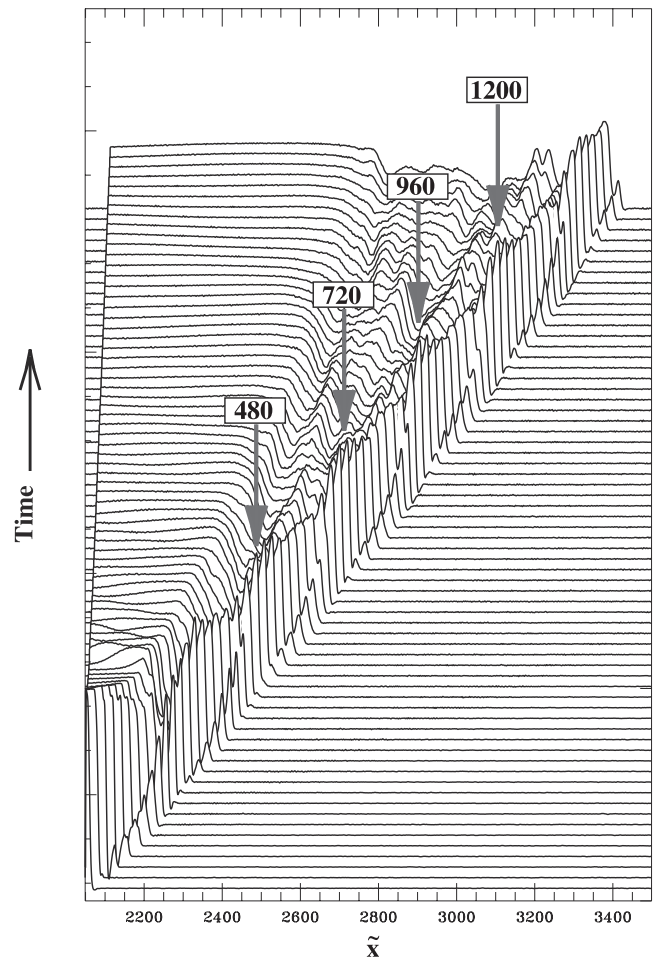


Figure 2. Stackplots of the y -averaged magnetic field B_{tz} at different times of the run. Cycles of the shock front reformation are illustrated by arrows which correspond to times where B_{tz} is maximum at the overshoot (the cyclic period is $\tilde{T}_{ref} \approx 240$). Propagation angle is $\theta_o = 55^\circ$.

the shock front is the source of the shock front nonstationarity and is characterized by a time period T_{refs} which is of the order of the ion gyroperiod calculated from the mean value of the magnetic field in the ramp. Cycles are indicated by arrows in Figure 2. Front reformation has the following consequences: (1) the amplitude of the overshoot is modulated in time and exhibits a minimum value within each cycle and (2) the width of the total shock front (including the ramp and the foot) is slightly varying in time. Similar shock reformation is also evidenced for each electromagnetic and electrostatic field component. As a consequence, the gradient of the main electrostatic field in the shock ramp is varying in time and may affect the interaction of electrons with the shock front and the resulting electron heating.

3.2. Nonuniformity of the Shock Front

[11] The shock front is not homogeneous as shown in Figure 3, and exhibits a rippling already analyzed by *Lembège and Savoini* [1992]. The precise identification of waves responsible for the rippling for different θ_0 is beyond the scope of the current paper. Since this rippling propagates along y axis, it leads to a second source of nonstationarity in the shock front; the characteristic timescale is much lower than the ion gyroperiod. This nonuniformity and nonstationarity character takes place in the entire shock front, that is, both in the ramp and the foot, and is always present in time. Similar results are also evidenced in the 3-D plots of all electrostatic and electromagnetic field components (not shown herein).

[12] Then, the following questions arise: what are the respective width scales of both magnetic and electrostatic field components, and how these scales are respectively affected by the nonuniformity and the nonstationarity of the shock front?

3.3. Scales of Fields Components

[13] In order to answer these questions, three different statistical studies on the B_{tz} and E_{lx} fields scales have been performed respectively (1) at a given time (nonuniformity effects included only), (2) at given y (nonstationary effects included only), and (3) when both effects are included. The procedure used for the precise measurements of spatial widths of E_{lx} and B_{tz} fields in the ramp (respectively L_{Er} and L_{Br}), and statistical results have been already presented in Figures 1 and 2 of *Lembège et al.* [1999]. The overall statistics obtained for case 3 are illustrated in Figure 4. It should be noted that both the width of the magnetic field ramp and the width of the region in which the largest change in the electric field is observed show similar distributions. These distributions have mean values of 8.75 and 10.2 and standard deviations of 4.1 and 3.6, respectively. In short, the width of the magnetic ramp was determined to be the region in which the magnetic field exhibits a large, constant gradient. The width of the electric field signature was calculated as being the distance between the onset and cessation of the constant gradient observed on either side of the U-shaped feature in the electric field. However, because of the dynamics of the ramp, it was sometimes difficult to distinguish the limit between the foot and the ramp and hence would result in an underestimate of L_{Br} ; this can account for the large R -values found in the tail of the distribution, where $R = L_{Er}/L_{Br}$.

[14] In all of the cases (1–3) mentioned above, the width of the E_{lx} is found to be comparable to that of B_{tz} (at least in the present moderate supercritical Mach regime) so that ratio R presents a peak around 1 (Figure 4). This width is always between the electron and the ion inertia lengths. The broadening observed in the statistical R -distribution is due to nonuniform and nonstationary effects. It should be noted that present simulations are based on the use of nonrealistic mass ratio because of numerical constraints. Such a low ratio compresses the range of lengths. However, recent 1-D full particle simulations [*Scholer et al.*, 2003] based on a realistic mass ratio confirm that the ramp thickness L_{Br} of the magnetic field can be quite narrow ($L_{Br} \approx$ a few c/ω_{pe}) and that $R \approx 1$ persists even when $M_i/m_e = 1846$. In conclusion, both results issued from 1-D and 2-D simulations seem to be consistent with $R \approx 1$. To the knowledge of the authors, no 2-D full particle simulations using a realistic mass ratio have been done yet.

3.4. Comparison Between Full Particles and Hybrid Simulations

[15] It is important to stress that the present results have not been observed in previous hybrid simulations where ion scales are fully included but electron scales are neglected. In such codes, the smallest physical scale to be accessed by the shock ramp was restricted to the ion inertial length, and the spatial resolution was limited so that $c/\omega_{pi} \approx 1-2\Delta$ where Δ is the space grid size. Only recently, results from 1-D hybrid simulations by *Hellinger et al.* [2002] have recovered a ramp thickness much lower than c/ω_{pi} , and a self reformation of the shock front similar to that of present Figure 2, provided that a high spatial resolution is used ($c/\omega_{pi} \gg \Delta$). However, these latest works have not provided yet any values for the scale widths L_{Br} and L_{Er} . In full particle code where both ion and electron scales are fully involved, the width of the ramp may access self consistently to physical scales much less than the ion inertial length and larger than electron inertial length (since $\Delta \ll c/\omega_{pe} \ll c/\omega_{pi}$). In addition, resistive effects including electron scales are fully described in 2-D full particle simulations in contrast with hybrid simulations where resistivity is described by a phenomenological constant.

3.5. Comparison With Previous Direct and Indirect Experimental Measurements

[16] The measurement of the characteristic width L_{Br} has been the subject of numerous previous investigations. The influence of the various physical processes on shock scales has been reviewed by *Kennel et al.* [1985]. Both *Scudder et al.* [1986a] and *Newbury and Russell* [1996] estimated the scale of the magnetic ramp as $0.2c/\omega_{pi}$ and $0.05c/\omega_{pi}$ respectively. The latter case corresponds to an unusually very thin shock. The determination of ramp scales for the 11 quasiperpendicular shocks, measured by OGO-5 and ISEE-1 and 2, was made by *Balikhin et al.* [1995]. It was shown that for all 11 shocks the size of the ramp was smaller than c/ω_{pi} . Among these 11 shocks, four have magnetic ramp scales even $< 0.15c/\omega_{pi}$.

[17] One important question is to determine the spatial width of the electrostatic field variation within the ramp. The different types of observations, where L_{Er} is smaller, comparable to, or larger than L_{Br} have been summarized in

$B_{tz}(x,y)$

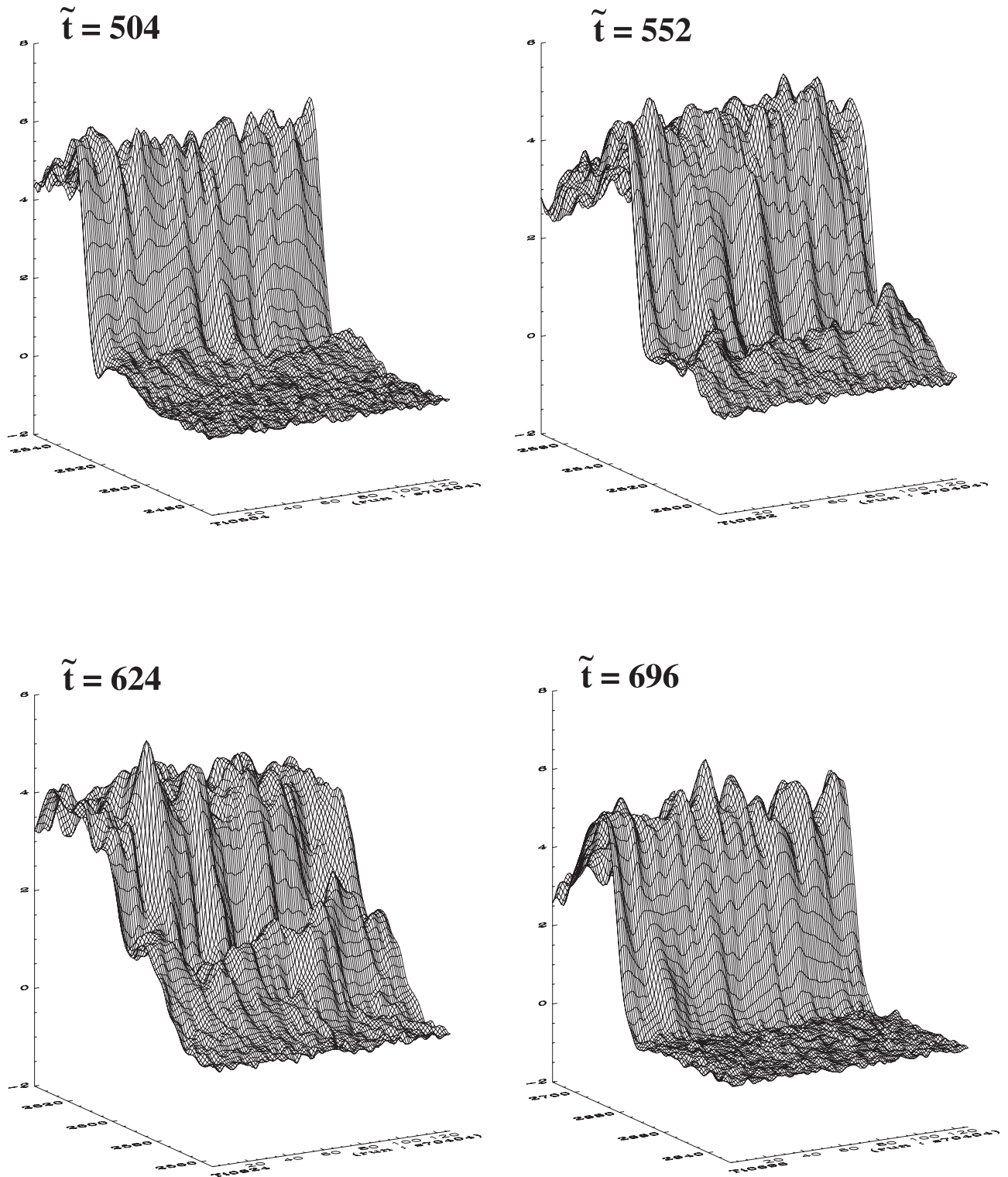


Figure 3. Three-dimensional plot of the B_{tz} magnetic field component measured at different times of the run chosen within a cyclic reformation period range, respectively $\tilde{t} = 504, 552, 624$ and 696 , (i.e., respectively $\tilde{t} = 0.96, 1.05, 1.19$, and $1.33 \tilde{\tau}_{ci}$).

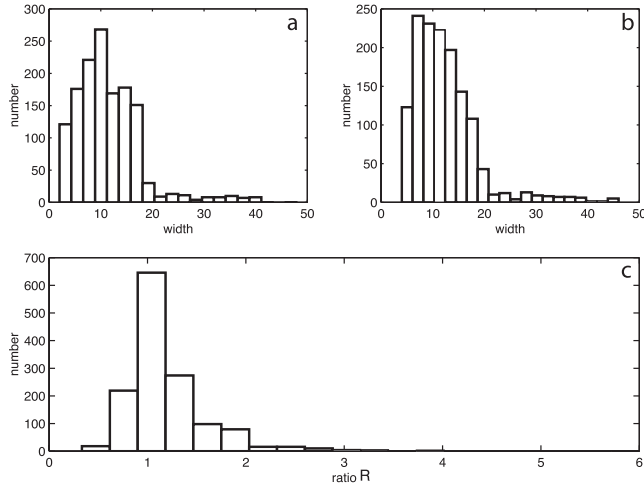


Figure 4. Effects of both nonstationarity and nonuniformity of the shock front. Statistical results are made on the width of the magnetic ramp L_{Br} (Figure 4a) of the electrostatic ramp L_{Er} (Figure 4b), and on their ratio $R = L_{Er}/L_{Br}$ (Figure 4c). Results are from the 2-D simulations obtained for $\theta_o = 55^\circ$.

previous works [Lembège *et al.* [1999]. For the case $L_{Br} \approx L_{Er}$ of interest herein, one of the most accurate direct determinations of the electric field potential change at the front of the Earth's bow shock has been made by Formisano [1982], using data from the ISEE electric field experiment. It was found that the temporal (i.e., spatial) scales of the potential change and of the magnetic ramp are of the same order. This conclusion is also valid for the other supercritical quasiperpendicular shocks reported by Formisano and Torbert [1982]. In addition, recent experimental observations from Cluster-2 also evidence that the spatial widths of B_{tz} and E_{lx} fields measured in the ramp are comparable (Figure 3 of Balikhin *et al.* [2002]).

[18] All of these experimental observations and numerical results indicate that $R \approx 1$. As a consequence, the demagnetization of electrons is expected to occur within the first part of the ramp; if confirmed, this demagnetization can be used to account for the deviation from adiabaticity through the shock front [Balikhin *et al.*, 1989, 1993, 1998; Krasnoselskikh *et al.*, 1995].

4. Comparison Between Theoretical and Numerical Results

4.1. Summary of Previous Theoretical Analysis

[19] The motivation of the present study is initially based on a controversy between theoretical and experimental approaches. First, let us remind that adiabaticity is related to magnetized particles, that is, to particles having many gyrations during their crossing of the shock ramp ($r_L \ll L_{Br}$ where r_L is the Larmor radius). In other words, adiabaticity applies to particles having relatively small thermal velocity ($v_{the} \ll L_{Br} \omega_{ce}$), that is, weak bulk motion since $V_{bulk} \ll v_{the}$. This theoretical argument is in disagreement with the content of Figure 7 of Schwartz *et al.* [1988], which shows that adiabatic and nonadiabatic heating takes place respectively for V_{bulk}/v_{the} smaller and larger than 0.18. In other words, nonadiabatic heating is evidenced even within a noticeable

range of the ratio $V_{bulk}/v_{the} \ll 1$. Then, one wonders whether the effect of the electric field at the ramp may account for this discrepancy.

[20] Let us be reminded that in the presence of the electric field gradient, the effective gyrofrequency ω_{eff} of a particle differs from the magnetic gyrofrequency ω_{ce} [Cole, 1976] as

$$\tilde{\omega}_{eff}^2 = \tilde{\omega}_{ce}^2 - \frac{d\tilde{E}_x}{d\tilde{x}} \quad (1)$$

in our normalized parameters. Balikhin *et al.* [1998] applied this result to electrons, and stressed out that change of the effective gyrofrequency leads to a change of the effective gyration radius $R_{eff} = v_{th}/\omega_{eff}$. If the gradient of the electric field is positive and its absolute value approaches some threshold (ω_{ce}^2), the effective gyrofrequency ω_{eff} is near zero, and R_{eff} tends to an infinite value. This means that the scanning of the shock ramp by the electron gyromotion may drastically change according to the local strength of the dE/dx gradient with respect to that of the local B field. In presence of a strong electric field gradient, electrons will be demagnetized even for a large but finite thickness of the shock front. In other words, a very thin ramp in the shock front is not a necessary condition for demagnetization. As established by Balikhin *et al.* [1998] and Balikhin and Wilkinson [1996], if electron thermal velocity exceeds plasma bulk velocity $v_{the} \gg V_{bulk}$, there are three possible different regimes of the electron interaction with macroscopic field in the shock front (Figure 5).

[21] In the first case, $L_{Er} \gg L_{Br}$ [Scudder, 1995] and the electron motion can be described in a standard drift approx-

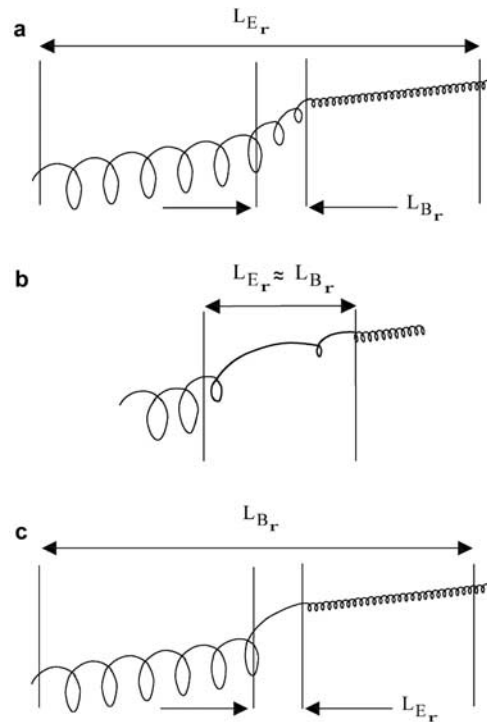


Figure 5. Sketch of an electron trajectory through the shock ramp according to the case (a) $L_{Br} \ll L_{Er}$, (b) $L_{Br} \approx L_{Er}$ and (c) $L_{Br} \gg L_{Er}$.

imation (Figure 5a). In such a case, an electron gyrates with a Larmor frequency and drifts because of the presence of electric field and of magnetic field gradient. The only increase of the electron energy is due to the gradient drift in the presence of electric field. Such a motion corresponds to a magnetized particle. Even in that case, the presence of a small gradient of the electric field results in some change of the gyrofrequency. The decrease of the electrostatic potential scale leads to the decrease of the electron gyrofrequency (deviation from the formally Larmor frequency calculated from the magnetic field only), and to the increase of the gyration radius. In the second case (Figure 5b), $L_{Er} \approx L_{Br}$. The effective Larmor radius is even larger and only one or two gyrations are performed by the electron during the ramp crossing; its motion within the ramp cannot be considered as magnetized any more. The imaginary part of the gyrofrequency increases with the decrease of the electrostatic potential scale and leads to the divergence of close electron trajectories in the velocity space and to some effective electron heating [Balikhin *et al.*, 1998]. The third case (Figure 5c), takes place when $L_{Er} \ll L_{Br}$; the particle is strongly demagnetized. The time of the ramp crossing does not need to be large enough for electron trajectories to diverge considerably, and electron heating at the shock front represents something like differential acceleration similar to the differential deceleration of ions in subcritical shocks [Balikhin and Wilkinson, 1996].

[22] These results emphasize the importance for determining correctly the spatial widths of both \vec{E} and \vec{B} fields at the shock ramp. From present numerical results, we have analyzed the conditions for which electron demagnetization may be evidenced and we have compared these conditions with theoretical predictions. Two different and complementary approaches are used: a self-consistent single particle approach (section 4.2) and a test particle approach (section 5).

4.2. Self Consistent Full Particle Results: A Single Particle Approach

[23] Results of section 3 have shown that the electron motion corresponding to the simulated shocks should correspond to the second case mentioned in section 4.1 (i.e., Figure 5b). As a consequence, demagnetization is expected in terms of particle trajectories. Present analysis is based on the use of “marked” electrons, which have interacted self-consistently with the fields and is summarized as follows: a first 2-D simulation run has been performed in conditions of section 2, from which results of section 3 have been issued. At a given time of the run ($\tilde{t} = 648$), we have marked several electrons located around the shock front including all those that have been reflected (**R**) and directly transmitted (**DT**). Then, a second longer run has been performed identical to the first one, in which we have followed and stored versus time velocity components ($\tilde{p}_x, \tilde{p}_y, \tilde{p}_z$), positions (x, y) of all marked electrons and all fields components seen by each of these electrons. Indeed, it is important to stress out that equation (1) [Cole, 1976] applies to fields and gradients of fields seen by the particle (not to be confused with the normal field plotted versus x). The time length of the run is long enough (until time $\tilde{t} = 1560$, that is, covering $3\tilde{\tau}_{ci}$) to identify easily **DT** and **R** electrons. Herein, we only focus our attention to **DT** electrons during their shock ramp crossing.

[24] Typical results are illustrated in Figure 6, which exhibits the features of one selected marked **DT** electron: the shock crossing occurs around time $\tilde{t} = 630$ (Figure 6a). While crossing the shock front, the electron suffers an important Y-drift (Figure 6b), which is related to the variation of both B_{tz} and E_{lx} fields components (Figures 6c and 6d). A simultaneous kinetic energy gain (mainly in the parallel energy) is evidenced at the shock front crossing (Figure 6e). Velocity component $\tilde{p}_{\perp 1}$ perpendicular to the local magnetic field shows time fluctuations of which timescale corresponds to local gyroperiod (Figure 6f). This period suffers combined effects of all \vec{E} and \vec{B} fields and associated gradients, allows to deduce the “full” electron gyroperiod $\tilde{\tau}_{full}$, and can be compared with theoretical predictions. On the same, the magnetic gyroperiod $\tilde{\tau}_{ce}$ has been deduced from the magnetic field versus time seen by the particle. Then, the time history of the local quantity $Q_{full} = 1 - (\tilde{\tau}_{full}/\tilde{\tau}_{ce})$ can be estimated. Results are represented by stars in Figure 7 for three typical electrons illustrating different levels of demagnetization.

[25] In order to compare directly with theoretical results, one identifies the time ranges where the field E_{lx} varies noticeably during the shock crossing (in particular where $dE_{lx}/dx > 0$ in the ramp). Within each range, one calculates the mean value $\langle Q_{full} \rangle$ averaged over all local Q_{full} values. The time evolution of $\langle Q_{full} \rangle$, allows to identify the ranges where demagnetization is evidenced ($\langle Q_{full} \rangle \neq 0$) or not ($\langle Q_{full} \rangle \approx 0$). For each particle, the value $\langle Q_{full} \rangle \approx 0$ measured in the upstream region is used as a reference; space distribution of stars around this value illustrates the error range made on the measurements because of the natural plasma fluctuations (and the numerical noise of the full particle code).

[26] Figure 7a corresponds to the electron features of Figure 6. The perpendicular velocity component $\tilde{p}_{\perp 1}$ shows a mean zero value in the upstream region, with a weak change when the electron crosses the shock front (top panel). This weak change corresponds to ranges where $dE_{lx}/dx > 0$ (for instance $577 < \tilde{t} < 634$). In addition, the value $\langle Q_{full} \rangle$ stays around zero everywhere, which means that the electron is mainly magnetized (bottom panel).

[27] Figure 7b illustrates the case where the mean value $\langle \tilde{p}_{\perp 1} \rangle$ differs from zero at the shock front and in particular in time range where $dE_{lx}/dx > 0$ ($614 < \tilde{t} < 633$). This $\tilde{p}_{\perp 1}$ drift is related to a shift independent of the magnetic field (which only leads to a change of ω_{ce}) and may be associated to the E_{lx} field effect (top panel). In addition, the mean value of $\langle Q_{full} \rangle$ noticeably differs from zero in the time range where $dE_{lx}/dx > 0$ ($\langle Q_{full} \rangle \approx -0.17$). This means that the demagnetization is not negligible any more (bottom panel).

[28] Figure 7c is analogous to Figure 7b but illustrates an even larger demagnetization ($\langle Q_{full} \rangle = -0.32$ for $593 < \tilde{t} < 615$ during the ramp crossing). This deviation is now illustrated by a large change in the mean value $\langle \tilde{p}_{\perp 1} \rangle$ exactly in the same time range (where $dE_{lx}/dx > 0$). The present demagnetization is relatively moderate since the Mach regime used herein has been chosen in order to correspond to moderate Mach regime observed in experimental data. It is evident that higher Mach regime will lead to higher fields gradients at the shock front and to a stronger demagnetization. The demagnetized particle performs about one rotation as it crosses the first half of the

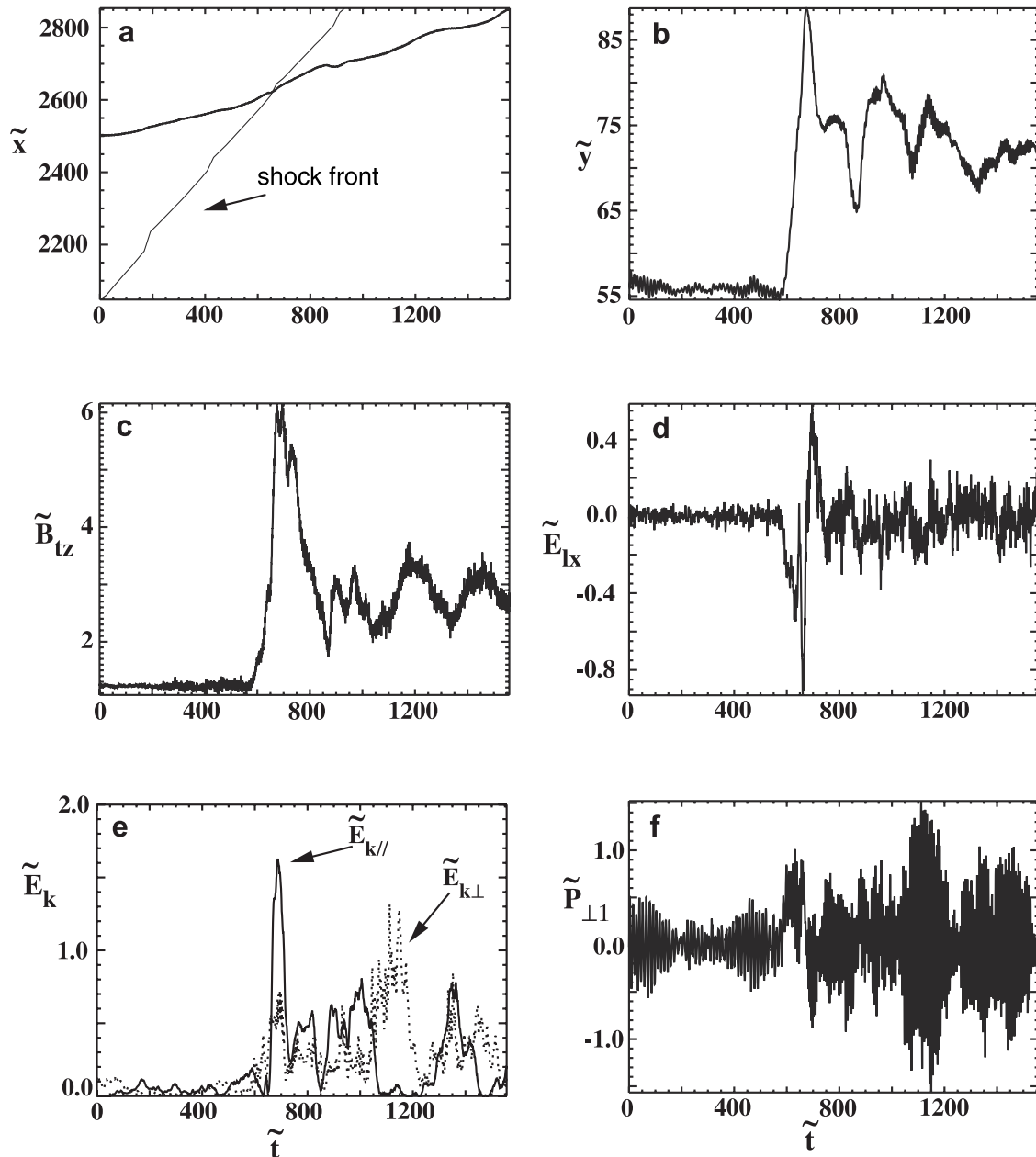


Figure 6. Main characteristics of one typical marked DT electron versus time: (a) x -coordinate of the particle (thick line) and mean x -position of the shock front (thin line) after averaging over y axis; (b) y -coordinate of the particle; (c) and (d) fields \tilde{B}_{tz} and \tilde{E}_{lx} seen by the electron; (e) parallel (full line) and perpendicular (dotted line) kinetic energy; (f) perpendicular velocity component $\tilde{p}_{\perp 1}$.

ramp ($dE_{lx}/dx > 0$). During this rotation time, the magnitude of the magnetic field increases almost twice. It is obvious that the main assumption of magnetization, that the scale of the electromagnetic field variations should be much higher than the spatial size of one gyroorbit, is not valid any more.

[29] It is important to stress that all three particles have almost similar x and y time trajectories (not shown here) when crossing the shock front. However, since these meet the shock front at different locations (both in x and y) and at different times, the \vec{E} and \vec{B} fields components seen by each particle (as in Figures 6c and 6d) differ from each other. Moreover, the effect of the other electrostatic component E_{ly} ,

is also fully involved in the self consistent particle trajectory. However, results cannot be compared with theory on this point since theoretical calculations do not include yet the effect of this component.

5. Test Particle Simulations Results

[30] At this stage, two questions are still unanswered. First, we ignore the electrons among an upstream distribution function that follow a demagnetized/magnetized motion during the shock front crossing. For so doing, we have to consider groups of electrons associated with same thermal velocity, located at exactly the same location from

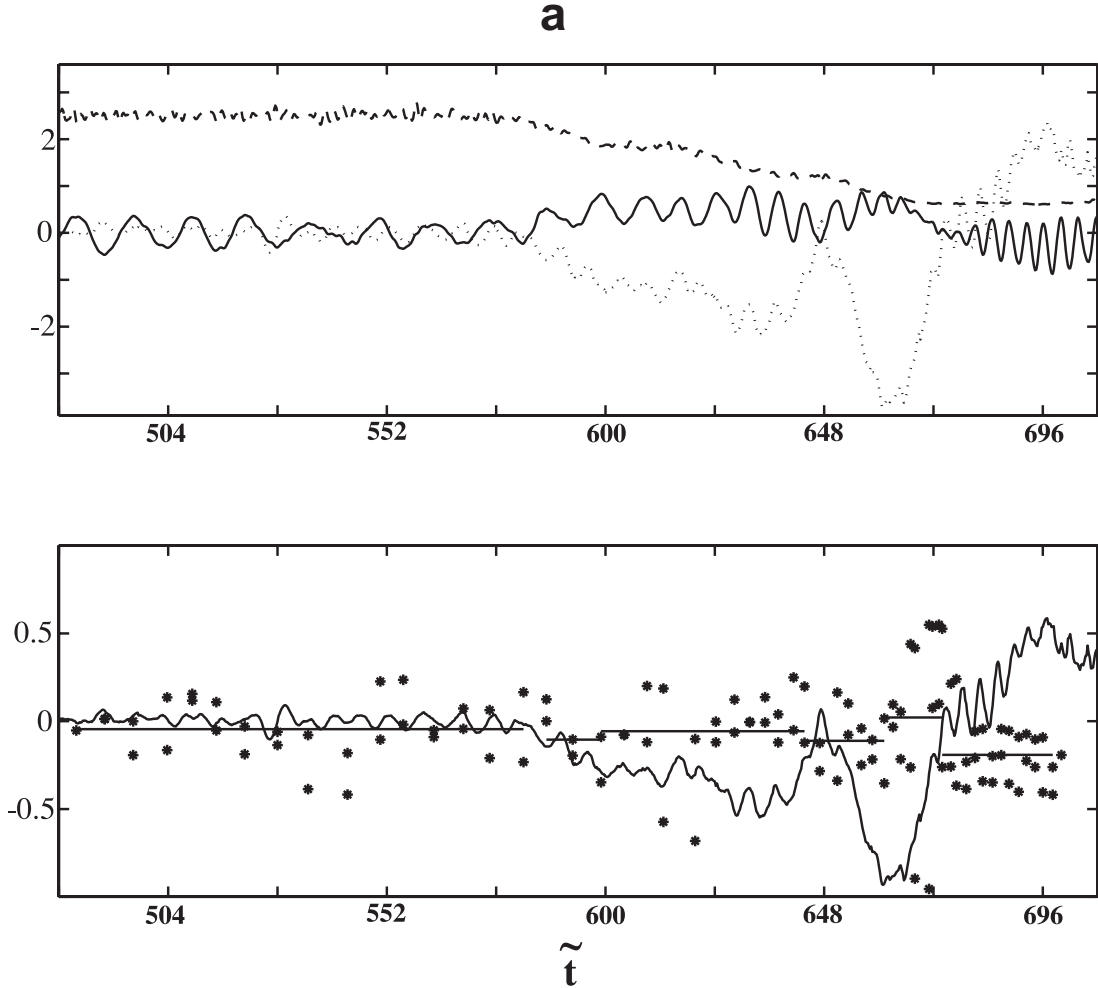


Figure 7. Time variation of features of three selected directly transmitted electrons. Two panels are dedicated to each particle. The top panel includes the electron gyroperiod $\tilde{\tau}_{ce}$ calculated from the variation of the magnetic field seen by the electron (dashed line), the electrostatic field \tilde{E}_{lx} seen by the electron (dotted line), and the perpendicular momentum component $\tilde{p}_{\perp 1}$ (full line). For the purpose of clarity, real values of $\tilde{\omega}_{ce}$, \tilde{E}_{lx} and $\tilde{p}_{\perp 1}$ have been multiplied by coefficients 0.2, 4, and 1, respectively. The bottom panel includes the electrostatic field \tilde{E}_{lx} seen by the electron (full line), which is used as a reference, local values of $Q_{full} = 1 - (\tilde{\tau}_{full}/\tilde{\tau}_{ce})$ represented by stars, and mean value $\langle Q_{full} \rangle$ locally averaged within some time ranges (see text). Results are only plotted within an enlarged time range around the shock front crossing made by each marked electron. Figures 7a, 7b, and 7c illustrate different levels of demagnetization (see text).

the front but having different phases in the velocity space. Identifying such electrons from self consistent simulation results is almost impossible. Second, we also ignore whether the nonhomogeneity and nonstationarity effects of the shock front contribute to the electron demagnetization. In order to clarify these two points, we have made use of test particle simulations in which electrons are interacting with a shock profile issued from the full particle simulations (shown in previous sections). Nonstationary and nonuniformity effects of the front have been removed, in order to focus only on the effects of spatial scales of fields components along x ; this allows a direct comparison with theory of *Balikhin et al.* [1998]. Profiles of all E and B components are chosen at a given time of the run, and are moving with a velocity v_{sh} along x identical to that measured in

section 4; at that time, an infinite homogeneous shock front is considered by using all fields y -averaged components. Electrons are distributed in velocity space over a cube (centered at the thermal velocity), which includes a set of 9 electrons (8 on each angle of the cube and 1 in the center). The side L_c of the cube is chosen relatively small with respect to the thermal velocity ($L_c = 0.001 v_{the}$) so that the estimated expansion coefficient can be compared with theoretical Lyapounov coefficient [*Balikhin et al.*, 1998]. Indeed, this last coefficient can be used provided that the deviation from the initial configuration is reasonable. In order to analyze the impact of the velocity phase, cubes are initially distributed uniformly with different phase angles Φ and Θ over a sphere in velocity space, whose radius is equal to the thermal velocity. For illustration, initial angular

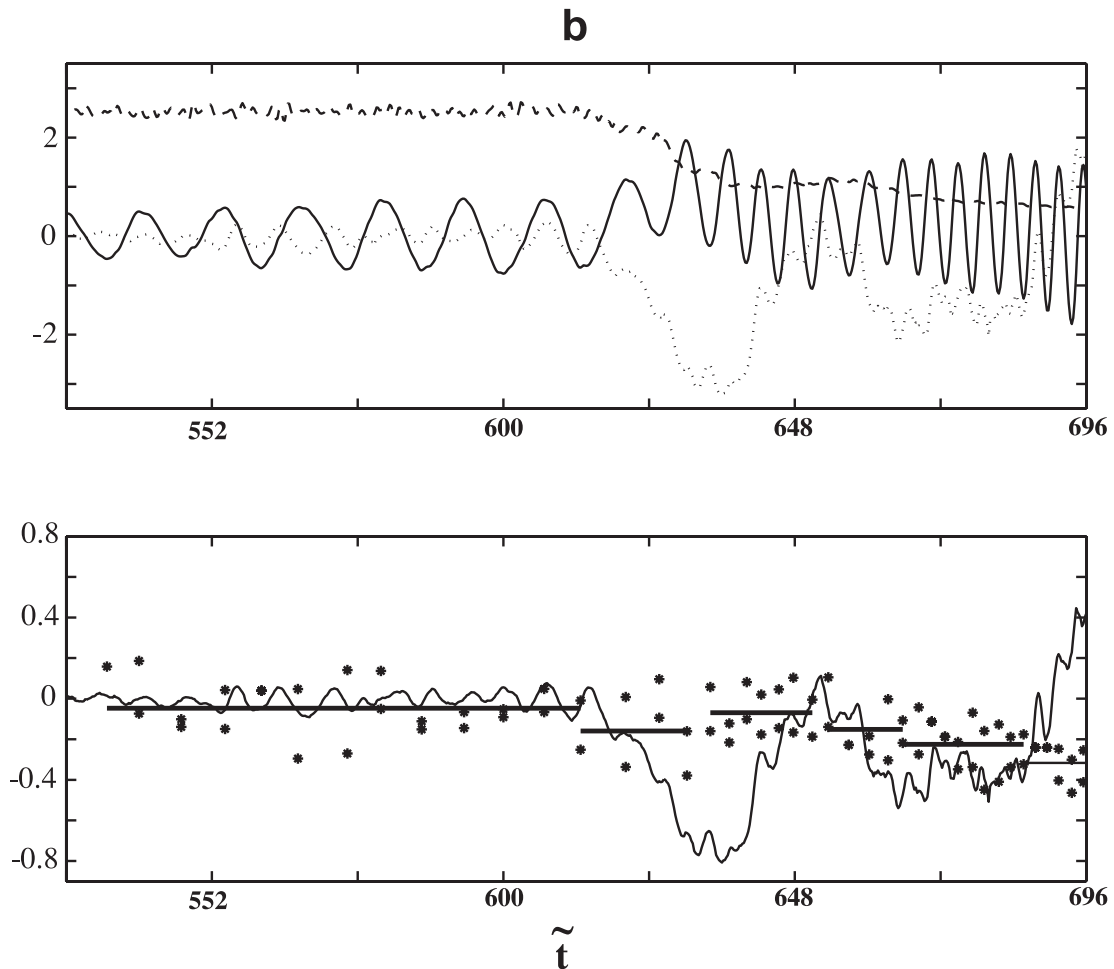


Figure 7. (continued)

locations of 20 cubes are represented in Figure 8a and will be used as reference in the following discussion. The center of the sphere is initially located upstream at a distance $\tilde{x} = 80$ from the ramp (Figure 8b).

[31] In the present case, we will analyze particle demagnetization by using three diagnosis sets: first, dynamics of the each barycentric electron (single test particle) and second, relative deformation of each cube (test particles cube). Several complementary diagnosis will be used in order to identify whether demagnetization takes place, its relative magnitude and the precise location of this deviation within the shock front. Third, a statistical analysis will determine the percentage of demagnetized/magnetized electrons according to their relative deviation based on the quantity $\langle Q_{full} \rangle$.

5.1. Single Test Particle Analysis

[32] For this study, the electron located at the barycenter of the cube will be considered as a reference particle. Several diagnosis are used: first, the time trajectory of the barycentric electron allows to evidence different types of interactions: some electrons are reflected (**R**), are directly transmitted (**DT**), or even do not interact with the front. In the latest case, electrons have the appropriate phase and a velocity large enough not to be overcome by the shock front

within the time range of concern. This means that the type of interaction strongly depends on the relative phase of the electron at the time of the shock front crossing. Presently, we focus our attention only on **DT** electrons. Second, the quantity $\langle Q_{full} \rangle$ directly provides a demagnetization estimate for the barycentric electron, similarly to the calculation performed for self-consistent particle in section 4.2. Third, the ratio $R_{full/eff} = 1 - (\tau_{full}/\tau_{eff})$ (where τ_{eff} may be estimated from equation (1)) will indicate the deviation of the full electron gyromotion as compared with theoretical effective gyromotion.

[33] Let us note that the use of magnetic momentum μ presents some risks. Deviation of the ratio $M (= \mu/\mu_o)$ from value 1 (where μ_o is the upstream momentum calculated at initial time $t = 0$) between upstream and downstream regions is often used to illustrate any possible deviation from adiabaticity. However, previous studies have clearly shown that adiabaticity behavior seems to prevail in situations where it is not expected (see the review of *Whipple et al.* [1986]). *Pesses* [1981] has shown in numerical simulations of particle motion through a perpendicular shock (of zero thickness), that the original magnetic momentum of a particle is often recovered by a particle after crossing the shock although it is violated during the transit. To the knowledge of the authors, the impact of the

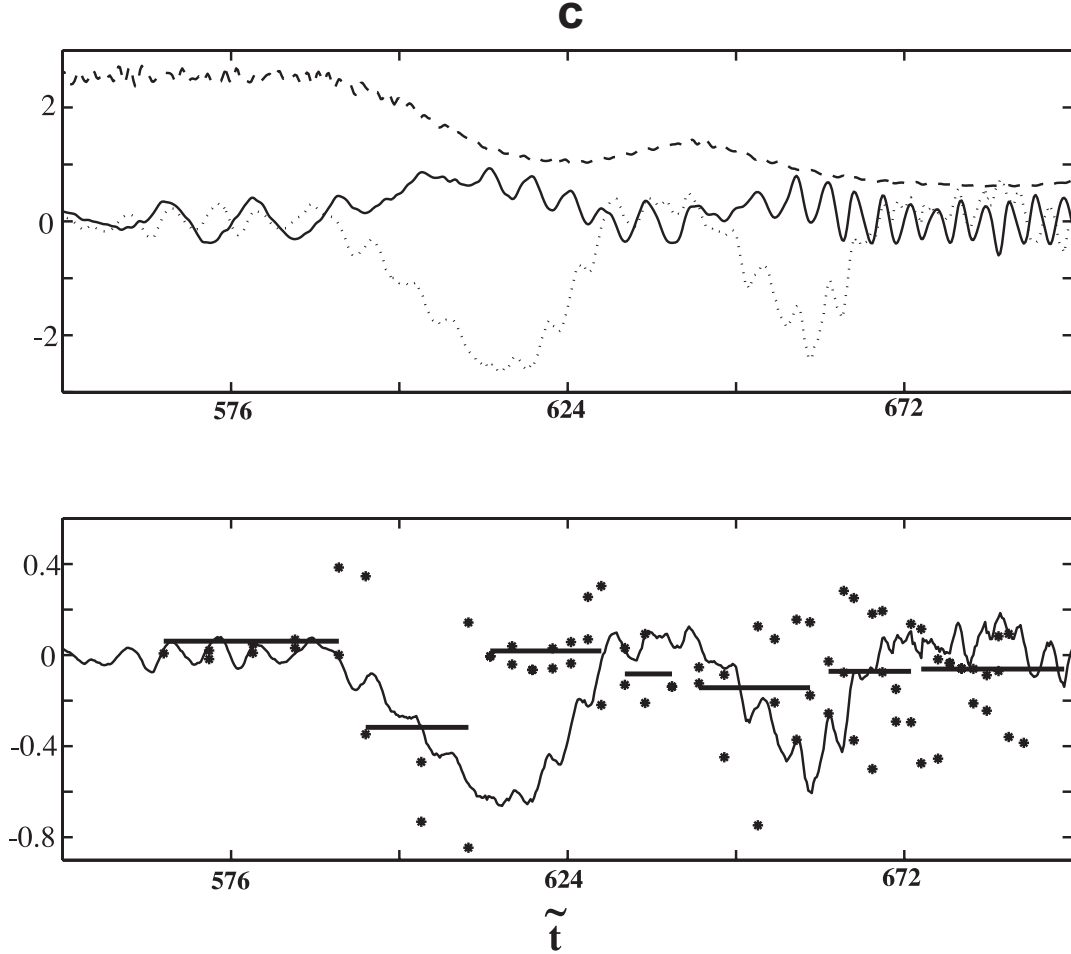


Figure 7. (continued)

finite front width on quantity M has not been analyzed yet. It is precisely the aim of this study to analyze where demagnetization take place within the shock front itself; then, the magnetic momentum μ will be not used herein.

[34] Numerical results are illustrated in Figures 9 (demagnetized electron) and 10 (magnetized electron). For each case, are represented time variations of the barycenter location and of main quantities necessary for its analysis. Because of their different phases, barycentric electrons cross the front with different velocities $v_{th,x}$ with respect to the direction of the shock front velocity v_{sh} along x . In the present case, most **DT** electrons (i.e., cubes 0 to 7, 11, 12 and 19) correspond to particles initially located in the half region of negative Θ (Figure 8a). All these electrons cross the shock front with initial pitch angle between 105° and 120° , that is, do have the appropriate phase for crossing the shock with velocity direction opposite to the front propagation.

[35] On the other hand, all **DT** electrons always see the same maxima values of E and B fields (which are stationary), but spend different time durations Δt according their phases when crossing the whole ramp. This affects their interaction with the ramp. The quantities $\langle Q_{full} \rangle$ and $R_{full/eff}$ will be quite different as confirmed by present results. We will focus on the time range $\Delta t_{>0} = t_B - t_A$

where the gradient dE_{lx}/dx is positive, that is, within the first part of the ramp. Main differences between demagnetized and magnetized electrons are summarized as follows:

[36] 1. Demagnetization is clearly identified by the noticeable deviation of the quantity $\langle Q_{full} \rangle$ from zero upstream value (Figure 9c) in contrast with Figure 10c. This deviation is always maximum exactly within $\Delta t_{>0}$ (Figure 9d). Weakly demagnetized electrons ($0 < |\langle Q_{full} \rangle| < 0.13$) correspond to barycenters 2, 4, 11 and 12. Noticeable demagnetization ($0.13 < |\langle Q_{full} \rangle| < 0.35$) is observed for barycenters 0, 1, 3, 5, 6, 7 and 19. The largest demagnetization ($|\langle Q_{full} \rangle| \approx 1.8$) is for barycenter 1. These results indicate that the demagnetization amplitude increases as Θ tends to -45° and Φ approaches large values ($|\Phi| > 90^\circ$).

[37] 2. Oscillations in E_{lx} , in the gradient dE_{lx}/dx and in B_{tz} time profiles seen by electrons illustrate the fact that the particle gyromotion forces the electron to see alternatively higher and weaker fields values during its ramp crossing. Such oscillations are quite clear for magnetized electron (Figures 10c–10d), but almost disappear in the time range $\Delta t_{>0}$ (i.e., where highest acceleration is expected) for the demagnetized electron (Figures 9c–9d), which suggests that the convection effect within the first part of the ramp is much stronger than gyromotion effect. Another clear evidence of demagnetization is also shown in x - y trajectories

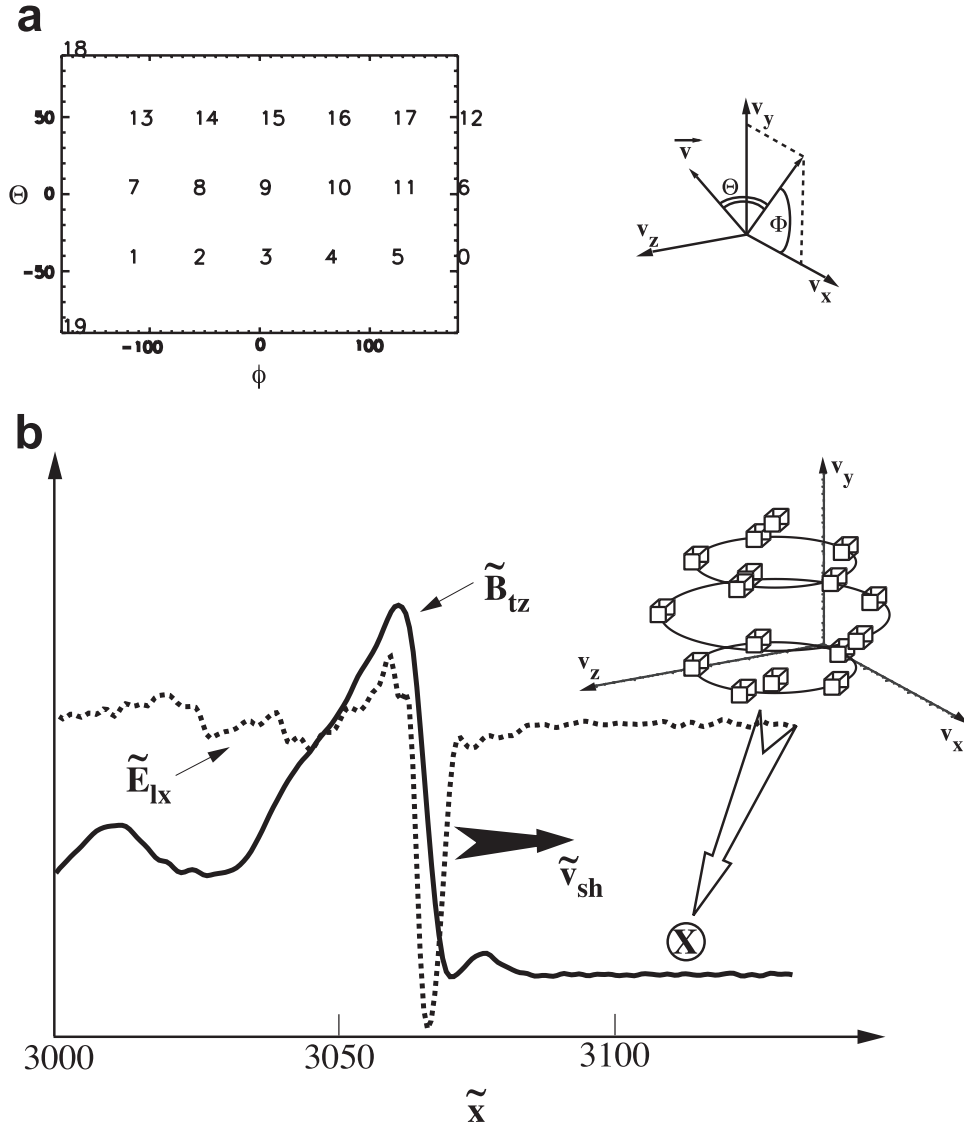
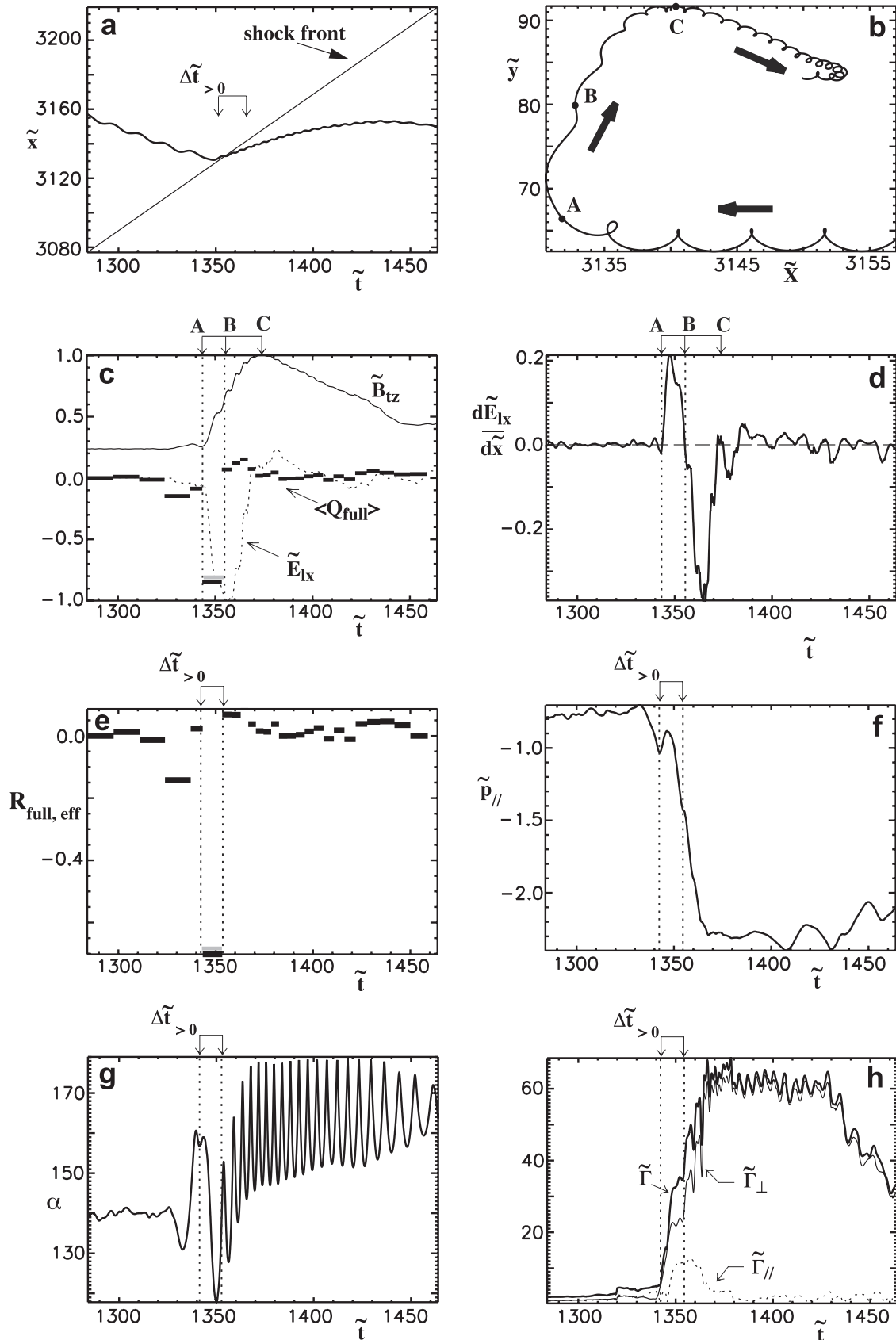


Figure 8. (a) Sketch of the cubes distribution over the sphere defined in the velocity space. Euler angles of the thermal velocity vector are defined by $\phi = (v_{th,x}, proj_{x,y}v_{th})$ and $\Theta = (proj_{x,y}v_{th}, v_{th})$. Each cube (i.e., barycentric electron herein) is identified by a number (0 to 19). (b) Profiles of the fixed B_{tz} and E_{lx} components, and location of the velocity sphere at initial time $t = 0$ of the test particle simulation; these profiles correspond to the y -integrated fields components measured at time $\tilde{t} = 1284$ in the 2-D full particle simulation.

(Figure 9b). The upstream gyromotion of the electron is replaced by a trajectory A-B strongly stretched along y axis within the range $\Delta t_{>0}$. This confirms the strong convection along y -direction which reduces the number of full gyrations as compared with a magnetized electron (Figure 10b).

Statistical analysis also shows that demagnetized electrons are characterized either by a y -deviation comparable (to that of the magnetized ones) but covered over a longer $\Delta t_{>0}$ (present case), either by a comparable $\Delta t_{>0}$ covering a longer y -deviation (not shown herein).

Figure 9. (opposite) Numerical results issued from test particles simulations for a typical demagnetized electron. Represented are the \tilde{x} -location of the barycenter (thick line) and of the shock front (thin line) versus time (Figure 9a), the time trajectory of the barycenter in the \tilde{x} - \tilde{y} plane (Figure 9b), the quantity $\langle Q_{full} \rangle$ (thick bars) with main fields components \tilde{E}_{lx} (dotted line) and \tilde{B}_{tz} (full line) (Figure 9c), the gradient $d\tilde{E}_{lx}/d\tilde{x}$ (Figure 9d), the quantity $R_{full,eff}$ (Figure 9e), the parallel momentum component \tilde{p}_{\parallel} (Figure 9f), the pitch angle α (Figure 9g) and the quantities Γ_{\parallel} , Γ_{\perp} , and Γ (Figure 9h). Figures 9c to 9h correspond to quantities seen by the barycentric electron versus time. The short time range $\Delta t_{>0} = t_B - t_A$ is defined from Figure 9d and is covered over the path A-B in Figure 9b; the large time range $\Delta t = t_C - t_A$ corresponding to the crossing of the whole ramp is measured from Figure 9c, is covered over the path A-C in Figure 9b and is reported in Figure 9d. The shock front is propagating with a velocity $\tilde{v}_{sh} = 0.73$ (from section 2).



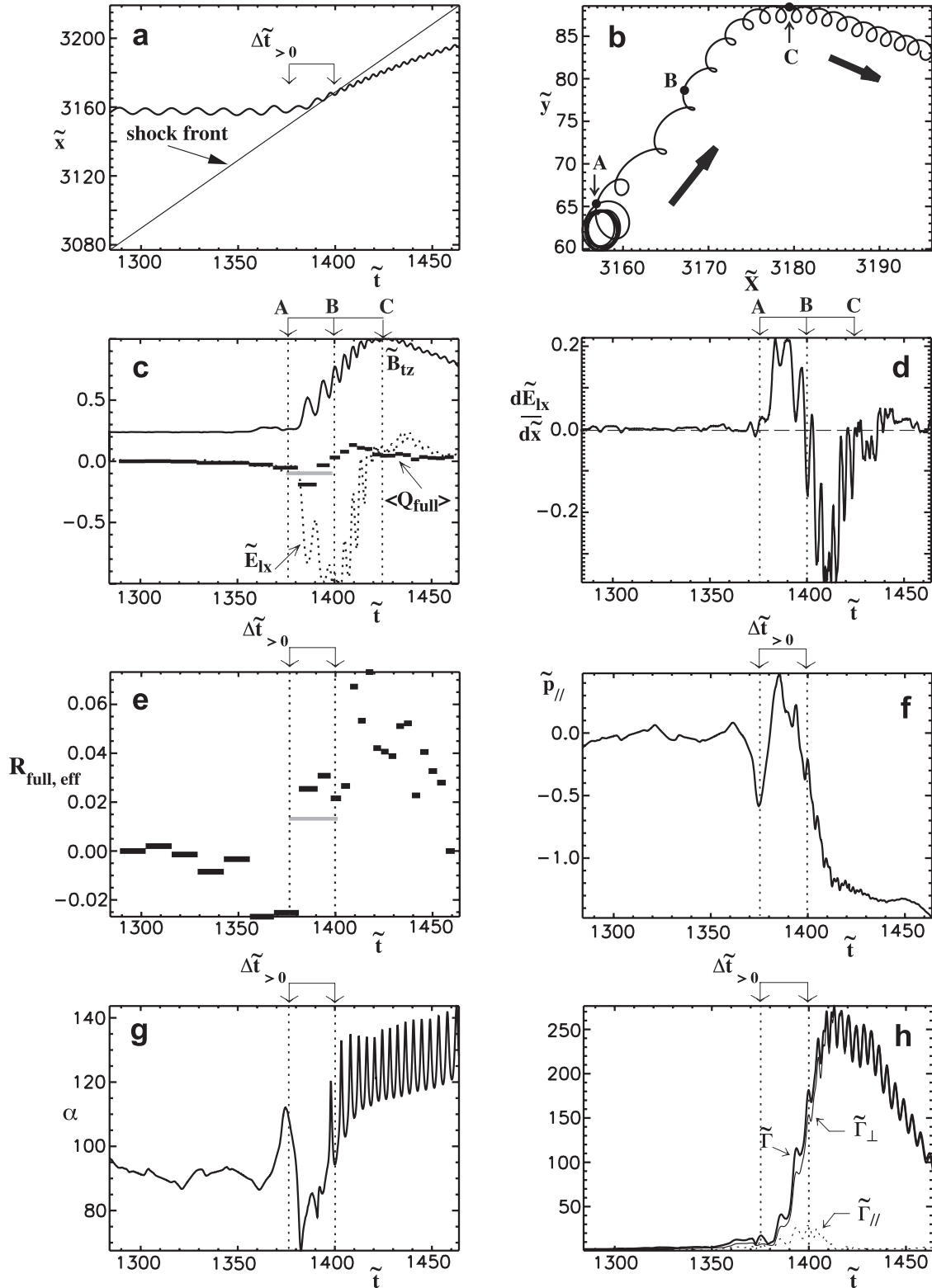


Figure 10. Same as Figure 9 for a characteristic magnetized barycentric electron.

[38] 3. Demagnetized electrons suffer a strong parallel acceleration within the time range $\Delta t_{>0}$ (Figure 9f). This acceleration still persists partially after $\Delta t_{>0}$ and reaches its highest value (saturation) at time the modulus of negative dE_{1x}/dx reaches its maximum. These electrons may stream

along the B field with a parallel velocity higher than magnetized ones, when penetrating the downstream region, as evidenced by comparing Figures 9f and 10f. In contrast, the magnetized electron suffers some deceleration and $p_{||}$ oscillates around zero value (bouncing effect) within the

range $\Delta t_{>0}$, so that its resulting energy gain is relatively limited (Figure 10f).

[39] 4. For demagnetized electrons, the pitch angle α only shows one large fluctuation within $\Delta t_{>0}$ (amplitude of 20°) around its upstream value (Figure 9g). When entering within the range where dE_{ix}/dx is negative, α increases with many fluctuations (13° amplitude) until reaching a saturation level (163° herein). No noticeable difference appears for the magnetized electron (Figure 10g), except that now the large amplitude fluctuations combined with the initial value of the pitch angle allow to reach the value 90° within $\Delta t_{>0}$ (bouncing effect).

[40] 5. Some demagnetized electrons spend less time within the whole ramp (Figure 9c) than magnetized ones (Figure 10c), that is, the time range where these suffer the effect of E_{ix} field is smaller. However, this is not always the case. This means that the estimate of this time range is not the main criteria for separating magnetized and demagnetized electrons. All crossing electrons see the same maximum value of gradient dE_{ix}/dx . Then, according to the theory of *Balikhin et al.* [1998], one would expect $\langle Q_{full} \rangle$ to be of similar amplitude, which is not the case. This apparent contradiction can be clarified by emphasizing that the time profile of dE_{ix}/dx is slightly different (in terms of local fluctuations) within $\Delta t_{>0}$ between demagnetized electrons according to their initial phase. Similarly, maxima values reached by $R_{full/eff}$ also vary within the range $\Delta t_{>0}$.

[41] Then, the present results confirm that demagnetization of electrons take place mainly within the first part of the ramp, in a good agreement with theoretical calculation of *Balikhin et al.* [1998]. However, further improvements of the theory is still necessary for estimating more precisely this deviation. This point is reinforced by the fact that $R_{full/eff}$ (Figure 9e) is always negative for demagnetized electrons within $\Delta t_{>0}$, which means that the theoretical frequency ω_{eff} overestimates the real frequency ω_{full} . The strong deviation of $R_{full/eff}$ (-0.68) within the range $\Delta t_{>0}$ means that the positive gradient dE_{ix}/dx cannot account alone for the full demagnetization of electrons. Other mechanisms not identified yet are also expected to contribute to this demagnetization.

5.2. Test Particle Cubes Analysis

[42] When crossing the shock front, a given cube is progressively deformed and one can follow this deformation in time. Barycenter and center of the cube are mixed at initial time $t = 0$ only. The deformation is calculated (1) first, by estimating the parallel and perpendicular velocity components for each of the 9 electrons, and (2) second, by measuring the time variation of the relative distance of each electron with respect to the barycenter. This procedure allows to estimate a coefficient of relative expansion (or shrinking) of the initial cubic structure respectively for parallel and perpendicular velocity directions; these coefficients are respectively defined by Γ_{\parallel} and Γ_{\perp} .

[43] For magnetized electrons, the expansion is mainly perpendicular; within the time range $\Delta t_{>0}$, Γ_{\parallel} is negligible ($\Gamma_{\parallel}/\Gamma_{\perp} \approx 13.8\%$ in Figure 10h). The total rate Γ follows roughly the B field variation within the front. Time variation of the expansion rate strongly varies from one cube of magnetized electrons to another. In contrast, the cube of demagnetized electrons exhibits some persistent features

(Figure 9h). First, even if Γ_{\parallel} still stays weaker than Γ_{\perp} , it is relatively much larger within the range $\Delta t_{>0}$ ($\Gamma_{\parallel}/\Gamma_{\perp} \approx 43\%$ in Figure 9h). This parallel expansion is a consequence of the strong parallel acceleration that each electron of the cube suffers. Second, the increase of the total rate Γ is more restricted within $\Delta t_{>0}$ for most demagnetized electrons than for the magnetized ones. Third, for the demagnetized case, the growth rate of Γ is the quickest only within the part of the time range $\Delta t_{>0}$ where the gradient dE_{ix}/dx increases, and starts saturating as dE_{ix}/dx starts decreasing. This result suggests that at least the second derivative of E_{ix} may have some impact on the demagnetization within $\Delta t_{>0}$.

[44] All the results are in agreement with theoretical prediction of *Balikhin et al.* [1998]. Main differences between magnetized and demagnetized electrons take place within the first part of the ramp as expected. However, this agreement is only qualitative but not quantitative. Indeed, maximum value of total Γ reached for demagnetized electrons within $\Delta t_{>0}$ is comparable to or even much less (present case) than that reached for magnetized ones. In all cases, it is never larger than that defined for magnetized electrons as expected from theoretical considerations [*Balikhin et al.*, 1998]. Present results suggest that this theory overestimates the demagnetization in terms of time expansion rate, and requires further improvement.

5.3. Test Particle Analysis: A Statistical Study

[45] Statistical analysis has been performed with 580 electrons (barycenters) distributed over the whole sphere in velocity space. The sphere is initially located far from the shock front at $\tilde{x} = 80$; 302 electrons are directly transmitted (**DT**). Demagnetized electrons are identified from the deviation of $|\langle Q_{full} \rangle|$ quantity from zero value within the time range $\Delta t_{>0}$. Results are illustrated in Figure 11a, where the fields components of the shock profile are issued from the same full particle simulation at time $\tilde{t} = 1284$. It is important to note that, when started at $\tilde{x} = 80$, all **DT** electrons suffer the effects of both the precursor and the ramp. Let us remind that the precursor is responsible for electron preheating, which can affect upstream electrons before crossing the ramp [*Savoini and Lembège*, 1995]. In the present case, the precursor is formed by the contribution of both the whistler precursor and the partial formation of the foot. Results clearly evidence that most **DT** electrons are demagnetized ($0.8 > |\langle Q_{full} \rangle| > 0.1$). A small percentage of electrons are strongly demagnetized ($|\langle Q_{full} \rangle| > 0.8$). In order to clarify the relative contribution of the ramp and of the precursor to the electron demagnetization, we have performed another identical run except that the sphere is now located very near the ramp at $\tilde{x} = 13$ (Figure 11a). Of course, this last run has no full physical meaning since it neglects any preheating effect but the procedure has the advantage of relative simplicity for a comparison of both cases. Number of **DT** electrons decreases from 302 to 290. It appears that (1) a noticeable percentage of electrons are still demagnetized within the ramp for $\tilde{x} = 13$ and (2) the demagnetization is stronger for electrons, which have interacted with both the precursor and the ramp ($\tilde{x} = 80$). In other words, the precursor deforms the velocity sphere (i.e., amplitude of the thermal velocity and phase of electrons in velocity space) before electrons reach the ramp in such a way to

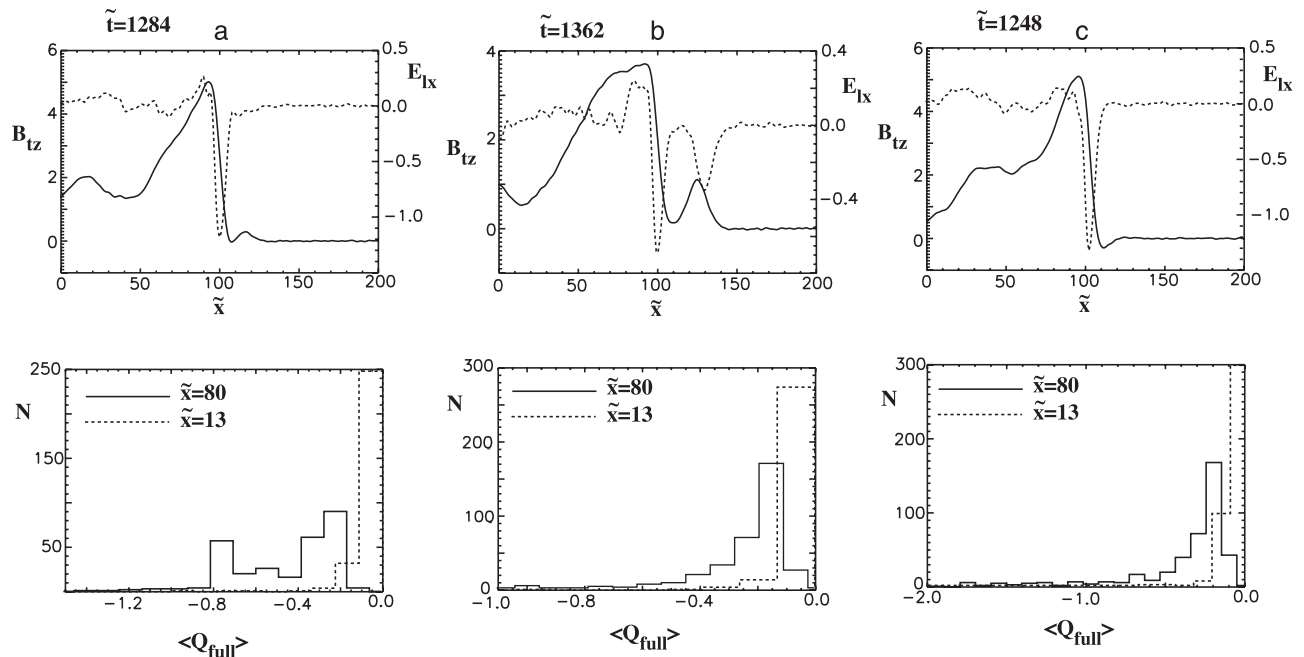


Figure 11. Top panels show profiles of \tilde{B}_{tz} (full line) and \tilde{E}_{lx} (dotted line) fields components at three different times $\tilde{t} = 1284, 1362$ and 1248 ; these profiles are y -averaged fields components issued from 2-D full particle simulations. Bottom panels show statistics of electrons versus the quantity $\langle Q_{full} \rangle$ averaged within the time range $\Delta t_{>0}$ of the shock ramp crossing, where $Q_{full} = 1 - (\tilde{\tau}_{full}/\tilde{\tau}_{ce})$ is calculated as in Figure 7; these results are issued from test particle simulations based on the fields components profiles defined in the corresponding top panels.

increase the resulting demagnetization. Another effect is that the precursor contributes to get more electrons transmitted through the shock front.

[46] Since the shock front is strongly nonstationary, one can expect that present statistical results may strongly vary for different profiles of E and B components measured at different times. In order to verify this point, two complementary test particle runs have been performed similar to that of Figure 11a, except that the used profiles of E and B components are now measured at times $\tilde{t} = 1362$ and 1248 .

[47] First, let us consider Figure 11b for which the precursor is mainly dominated by the foot. The foot amplitude is much larger and the ramp amplitude has decreased with respect to time $\tilde{t} = 1284$. The velocity sphere is unchanged, and is located at $\tilde{x} = 80$ and 13 . For $\tilde{x} = 80$, main changes with respect to Figure 11a are summarized as follows: (1) the number of **DT** electrons has increased from 302 to 354; (2) a larger percentage of weakly demagnetized electrons is measured within the same range $0.35 > |\langle Q_{full} \rangle| > 0.1$; and (3) in contrast, a weaker percentage of demagnetized electrons is measured for larger deviation ($0.8 > |\langle Q_{full} \rangle| > 0.4$). Only a few electrons are strongly demagnetized ($|\langle Q_{full} \rangle| > 0.8$) as in Figure 11a. When the sphere is initially located at a short distance from the ramp ($\tilde{x} = 13$), the number of **DT** electrons has slightly decreased from 354 to 331. A noticeable number of demagnetized electrons is still measured through the ramp alone, but the number of magnetized electrons increases. Comparison of both cases $\tilde{x} = 13$ and 80 confirms that the strength of the demagnetization is reinforced when electrons also interact with the foot.

[48] Second, let us consider Figure 11c for which the precursor is mainly dominated by the electromagnetic whistler emitted from the ramp (weak effect of the foot). The ramp amplitude is now comparable to that at time $\tilde{t} = 1284$. Results are similar to those obtained for Figure 11b, except that the number of **DT** electrons has increased from 354 to 432 ($\tilde{x} = 80$), and from 331 to 408 ($\tilde{x} = 15$). A noticeable number of demagnetized electrons is always evidenced at the ramp, and the interaction of electrons with the precursor again leads to a stronger resulting demagnetization. In all three cases of Figure 11, let us note that the ratio $R \approx 1$.

[49] As a consequence, the relative percentage of demagnetized/magnetized electrons and the demagnetization strength are strongly dependent on the shock front turbulence. These results have to be compared with experimental measurements performed by multisatellites mission as Cluster2. This last step requires an important parametric study (including full nonuniformity and nonstationary effects), and a detailed statistical analysis of experimental data which are out of the scope of the present study.

6. Conclusions

[50] In contrast with previous works, breakdown of electron adiabaticity has been analyzed in details within the shock front itself and not in terms of quantities jump between upstream and downstream regions (as for instance with magnetic momentum). This approach allows to determine precisely the local physical mechanisms responsible for this deviation. To the knowledge of the authors, this is

the first quantitative study within the shock ramp itself. The deviation is based on particle trajectory analysis where demagnetization can be identified and precisely estimated within the ramp. The use of full particle simulations is necessary in order to access self-consistently to all physical electron and ion time/spatial scales inherent to the dynamics of the shock front. This is a necessary condition to analyze the full interaction of electrons with the shock front even if the dynamics of the shock is strongly dictated by ions. In order to complete this analysis, both self consistent full particle and test particles (not self-consistent) simulations have been used. The main results are as follows:

[51] 1. Present statistical analysis confirms that (1) the width of the magnetic ramp is always lying between c/ω_{pe} and c/ω_{pi} , and (2) the width of the electrostatic field in the shock ramp can be comparable to the magnetic ramp width (ratio $R \approx 1$). These features are in good agreement with recent experimental measurements made by Cluster 2 and with recent full particle simulation based on the use of a realistic mass ratio. The ratio value $R \approx 1$ is quite appropriate for providing particle demagnetization and resulting nonadiabatic heating in the ramp, as predicted by previous theoretical works.

[52] 2. In order to verify these theoretical predictions, a first approach has been based on self-consistent “marked” electrons issued from full particle simulations, where non-stationarity and nonuniformity of the shock front are fully included. Indeed, one needs to know at least and simultaneously (1) the local \vec{B} and \vec{E} fields (or more exactly the gradient dE_{ix}/dx) seen by each self-consistent particle and (2) the associated momentum component $p_{\perp 1}$ versus time. Key diagnostics such as the time histories of the $p_{\perp 1}$ component, and of the measured quantity $\langle Q_{full} \rangle$, confirm quite well that the electron demagnetization take place within the first part of the ramp where $dE_{ix}/dx > 0$ (characterized by the time range $\Delta t_{>0}$).

[53] 3. A second approach has been performed with test particles simulations in order to identify precisely the basic underlying mechanisms responsible for demagnetization within the ramp along the shock normal. Nonstationary and nonuniformity of the shock front have been removed. Electrons are distributed over a sphere so that velocity phase effects are fully included. Demagnetized electrons are identified from deviation of the averaged quantities $\langle Q_{full} \rangle$ (with respect to their zero upstream values), measured within $\Delta t_{>0}$. Three complementary analysis have been performed. First, a single particle analysis has shown that a demagnetized electron suffers (1) a strong deviation of $\langle R_{full,eff} \rangle$, (2) a net increase of the parallel momentum p_{\parallel} , and (3) convection effects much stronger than gyromotion effects. These dominant effects lead to a noticeable stretched motion along the y -axis and to very weak time fluctuations in the fields components. Second, it was also shown that a cube of demagnetized electrons has a non-negligible parallel expansion rate within $\Delta t_{>0}$, even if it stays lower than the perpendicular rate. This parallel rate is negligible for magnetized electrons. Third, a statistical analysis has shown that the relative percentage of demagnetized/magnetized electrons within $\Delta t_{>0}$ is strongly dependent on the nonstationary behavior of the shock front (self reformation), and that the precursor increases the strength of the resulting demagnetization (as compared to

that of the ramp alone). In all cases analyzed herein, a noticeable percentage of demagnetized electrons is always formed within the ramp itself. This percentage is expected to increase in shocks with higher Mach number, characterized by larger gradient dE_{ix}/dx .

[54] All these results confirm that electron demagnetization takes place within the time range $\Delta t_{>0}$ as expected from theoretical considerations. This demagnetization reveals to be a good candidate for accounting for nonadiabatic heating through a shock front [Balikhin *et al.*, 1998]. However, this demagnetization cannot be explained by the contribution of the gradient dE_{ix}/dx alone, and other mechanisms not identified yet also contribute. These results need to be compared with experimental measurements performed by multisatellites mission Cluster-2.

[55] **Acknowledgments.** This work was performed under the auspices of the International Space Science Institute (ISSI, Bern, Switzerland) which the authors thank for its hospitality and financial support. Simulation runs have been made at the IDRIS center (Orsay).

[56] Shadia Rifai Habbal thanks Pierluigi Veltri and another referee for their assistance in evaluating this paper.

References

- Balikhin, M. A., M. E. Gedalin, and J. G. Lominadze, A possible mechanism of electron heating in collisionless perpendicular shock front, *Nucl. Fusion*, 12, 663, 1989.
- Balikhin, M. A., M. E. Gedalin, and A. Petrukovich, New mechanism for electron heating in shocks, *Phys. Rev. Lett.*, 70, 1259, 1993.
- Balikhin, M., V. Krasnoselskikh, and M. Gedalin, The scales in quasi-perpendicular shocks, *Adv. Space Res.*, 15, 247, 1995.
- Balikhin, M. A., and W. Wilkinson, Ion heating in the ramp of quasi-perpendicular shocks, *Geophys. Res. Lett.*, 23, 1063, 1996.
- Balikhin, M. A., V. Krasnoselskikh, L. J. C. Woolliscroft, and M. A. Gedalin, A study of the dispersion of the electron distribution in the presence of e and b gradients: Application to electron heating at quasi-perpendicular shocks, *J. Geophys. Res.*, 103, 2029, 1998.
- Balikhin, M. A., et al., Observation of the terrestrial bow shock in quasi-electrostatic subshock regime, *J. Geophys. Res.*, 107(A8), 1155, doi:10.1029/2001JA000327, 2002.
- Biskamp, D., and H. Welter, Numerical studies of magnetosonic collisionless shock waves, *Nucl. Fusion*, 12, 663, 1972.
- Cole, K. D., Effects of crossed magnetic and spatially dependent electric fields on charged particle motion, *Planet. Space Sci.*, 24, 518, 1976.
- Formisano, V., Measurements of the potential drop across the Earth's collisionless bow shock, *Geophys. Res. Lett.*, 9, 1033, 1982.
- Formisano, V., and R. Torbert, Ion acoustic wave forms generated by ion-ion streams at the Earth's bow shock, *Geophys. Res. Lett.*, 9, 207, 1982.
- Goodrich, C. C., and J. D. Scudder, The adiabatic energy change of plasma electrons and the frame dependence of the cross-shock potential at collisionless magnetosonic shock waves, *J. Geophys. Res.*, 89, 6654–6662, 1984.
- Hellinger, P., P. Trávníček, and H. Matsumoto, Reformation of perpendicular shocks: Hybrid simulations, *Geophys. Res. Lett.*, 29(24), 2234, doi:10.1029/2002GL015915, 2002.
- Heppner, J. P., N. C. Maynard, and T. L. Aggson, Early results from isee-1 measurements, *Space Sci. Rev.*, 22, 777, 1977.
- Kennel, C. F., J. P. Edmiston, and T. Hada, A quarter century of collisionless shock research, in *Collisionless Shocks in the Heliosphere: A Tutorial Review*, *Geophys. Monogr. Ser.*, vol. 34, edited by R. G. Stone and B. T. Tsurutani, pp. 1–36, AGU, Washington, D. C., 1985.
- Krasnoselskikh, V., M. A. Balikhin, M. E. Gedalin, and B. Lembège, Electron dynamics in the front of the quasi-perpendicular shocks, *Adv. Space Res.*, 15, 239, 1995.
- Lembège, B., and J. M. Dawson, Self-consistent study of a perpendicular collisionless and nonresistive shock, *Phys. Fluids*, 30, 1767, 1987.
- Lembège, B., and P. Savoini, Non-stationarity of a 2-d quasi-perpendicular supercritical collisionless shock by self-reformation, *Phys. Fluids*, 4, 3533, 1992.
- Lembège, B., S. N. Walker, P. Savoini, M. A. Balikhin, and V. Krasnoselskikh, The spatial sizes of electric and magnetic field gradients in a simulated shock, *Adv. Space Rev.*, 24, 109, 1999.
- Leroy, M. M., C. C. Goodrich, D. Winske, C. S. Wu, and K. Papadopoulos, Simulation of a perpendicular shock, *Geophys. Res. Lett.*, 8, 1269, 1981.

- Montgomery, M. D., J. R. Asbridge, and S. J. Bame, Vela 4 plasma observations near the Earth's bow shock, *J. Geophys. Res.*, *75*, 1217, 1970.
- Newbury, J. A., and C. T. Russell, Observations of a very thin collisionless shock, *Geophys. Res. Lett.*, *23*, 781, 1996.
- Pesses, M. E., On the conservation of the first adiabatic invariant in perpendicular shocks, *J. Geophys. Res.*, *86*, 150, 1981.
- Savoini, P., and B. Lembège, Electron dynamics in two and one dimensional oblique supercritical collisionless magnetosonic shocks, *J. Geophys. Res.*, *99*, 6609, 1994.
- Savoini, P., and B. Lembège, Heating and acceleration of electrons through the whistler precursor in 1-D and 2-D oblique shocks, *Adv. Space Rev.*, *15*, 235, 1995.
- Schwartz, S. J., M. F. Thomsen, S. J. Bame, and J. Stansberry, Electron heating and the potential jump across fast mode shocks, *J. Geophys. Res.*, *93*, 12,923, 1988.
- Scholer, M., I. Shinohara, and S. Matsukiyo, Quasi-perpendicular shocks: Length scale of the cross-shock potential, shock reformation, and implication for shock surfing, *J. Geophys. Res.*, *108*(A1), 1014, doi:10.1029/2002JA009515, 2003.
- Scudder, J. D., A. Mangeney, C. Lacombe, C. C. Harvey, T. L. Aggson, R. R. Anderson, J. T. Gosling, G. Pashmann, and C. T. Russell, The resolved layer of a collisionless, high β , supercritical, quasi-perpendicular shock wave: 1. Rankine-Hugoniot geometry, currents, and stationarity, *J. Geophys. Res.*, *91*, 11,019, 1986a.
- Scudder, J. D., A. Mangeney, C. Lacombe, C. C. Harvey, and T. L. Aggson, The resolved layer of a collisionless, high β , supercritical, quasi-perpendicular shock wave: 2. Dissipative fluid electrodynamics, *J. Geophys. Res.*, *91*, 11,053, 1986b.
- Scudder, J. D., A review of the physics of electron heating at collisionless shocks, *Adv. Space Res.*, *15*, 181, 1995.
- Tokar, R. L., C. H. Aldrich, D. W. Forslund, and K. B. Quest, Nonadiabatic electron heating at high-mach-number perpendicular shock, *Phys. Rev. Lett.*, *56*, 1059, 1986.
- Veltri, P., A. Mangeney, and J. D. Scudder, Electron heating in quasi-perpendicular shocks: A Monte Carlo simulation, *J. Geophys. Res.*, *95*, 14,939, 1990.
- Veltri, P., and G. Zimbardo, Electron-Whistler interaction at the Earth's bow shock: 1. Whistler instability, *J. Geophys. Res.*, *98*, 13,325, 1993a.
- Veltri, P., and G. Zimbardo, Electron-whistler interaction at the Earth's bow shock: 1. Electron pitch angle diffusion, *J. Geophys. Res.*, *98*, 13,335, 1993b.
- Whipple, E. C., T. G. Northrop, and T. J. Birmingham, Adiabatic theory in regions of strong field gradients, *J. Geophys. Res.*, *91*, 4149, 1986.

M. Balikhin and S. Walker, Department of Automatic Control and Systems Engineering, University of Sheffield, Mappin Street, Sheffield S1 3JD, U.K. (balikhin@acse.sheffield.ac.uk)

V. Krasnoselskikh, Laboratoire de Physique et Chimie de l'Environnement, CNRS, 3a, Avenue de la recherche scientifique F-45071 Orléans la Source, France. (vkrasnos@cnsr-orleans.fr)

B. Lembège and P. Savoini, Centre d'Etude des Environnements Terrestre et Planétaires/Université de Versailles Saint-Quentin-en-Yvelines (CETP/UVSQ), 10-12, Avenue de l'Europe, F-78140, Vélizy, France. (bertrand.Lembege@cetp.ipsl.fr; Philippe.Savoini@cetp.ipsl.fr)